Silicon vacancy center in 4H-SiC: Electronic structure and spin-photon interfaces

Ö. O. Soykal, Pratibha Dev, and Sophia E. Economou

Silicon vacancy center in 4H-SiC: Electronic structure and spin-photon interfaces

Ö. O. Soykal,[1] Pratibha Dev,[1, 2] and Sophia E. Economou[3, 4]

[1]*NRC post doc residing at Code 6877 Naval Research Laboratory, Washington, D.C. 20375, USA*
[2]*Department of Physics and Astronomy, Howard University, Washington, DC, USA*
[3]*Naval Research Laboratory, Washington, DC 20375*
[4]*Department of Physics, Virginia Tech, Blacksburg, Virginia 24061, USA*

Defects in silicon carbide are of intense and increasing interest for quantum-based applications due to this material's properties and technological maturity. We calculate the multi-particle symmetry adapted wave functions of the negatively charged silicon vacancy defect in hexagonal silicon carbide via use of group theory and density functional theory and find the effects of spin-orbit and spin-spin interactions on these states. Although we focused on V_{Si}^- in 4H-SiC, because of its unique fine structure due to odd number of active electrons, our methods can be easily applied to other defect centers of different polytpes, especially to the 6H-SiC. Based on these results we identify the mechanism that polarizes the spin under optical drive, obtain the ordering of its dark doublet states, point out a path for electric field or strain sensing, and find the theoretical value of its ground-state zero field splitting to be 68 MHz, in good agreement with experiment. Moreover, we present two distinct protocols of a spin-photon interface based on this defect. Our results pave the way toward novel quantum information and quantum metrology applications with silicon carbide.

Over the last several years, deep-center defects in solids have been intensely researched for applications in quantum information [1, 2], quantum sensing and nanoscale imaging [3] including bioimaging [4, 5]. Their success and popularity stem from their unique properties, combining advantages from atomic and solid state systems-most notably long spin coherence times even at room temperature and integrability into a solid state matrix. The NV^- center in diamond is the most studied defect for quantum technologies, so that its properties, strengths and limitations are by now very well understood. Deep defect centers in silicon carbide (SiC) have emerged as strong contenders due to this material's significantly lower cost, availability of mature microfabrication technologies [6, 7], and favorable optical emission wavelengths [8].

Some of the stable defects in SiC have the same structure as the NV^- center in diamond in terms of symmetry and the number of active electrons and, as a result, spin and electronic structure. Such defects include the silicon-carbon divacancy, which has been investigated over the last several years [9–12]. Experiments [8, 13–18] on the Si *monovacancy* (V_{Si}^-) have shown that this is a distinct defect in terms of electronic and spin structure. It features a ground state with total spin 3/2 [13, 15], offering both quantitative improvements and qualitatively new capabilities [16] compared to NV-like defects. To date, room temperature spin polarization and coherent control of V_{Si}^- have been implemented via electron spin resonance [17, 19] and optically detected magnetic resonance (ODMR) [8, 15, 18, 20]. Unlike the well-studied NV^- center in diamond [21–23], theoretical studies of the V_{Si}^- in SiC have been mostly limited to finding single-particle levels and their energies via density functional theory (DFT) [24–26]. While such DFT calculations are an important first step, it is of crucial importance to obtain the multi-particle electronic structure to understand the properties of this defect and take full advantage of the novel opportunities it affords.
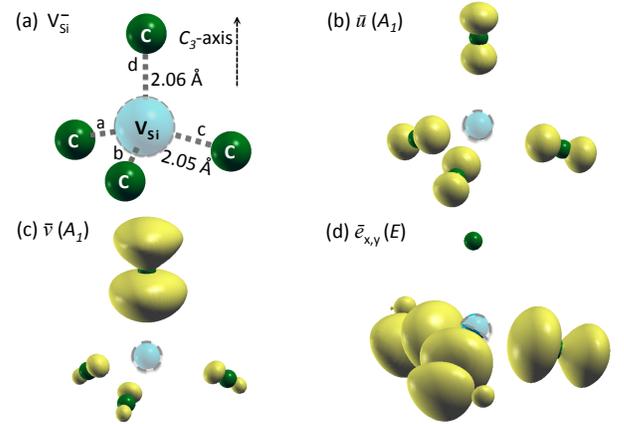
FIG. 1. (color online) V_{Si}^- in 4H-SiC: (a) $C_{3\nu}$-structure of the defect, and the optically-active orbitals of V_{Si}^- using DFT: (b) $\bar{u}$ (A_1 symmetry), (c) $\bar{v}$ (A_1), and (d) $\bar{e}_{x,y}$ (E). Only carbons near the V_{Si}^- are shown for clarity.

In this Letter we address this need by calculating the multi-particle wave functions of V_{Si}^- through a combination of group theory and DFT. We explicitly find the ground states as well as the excited state manifolds, considering both the orbital and the spin degrees of freedom. Furthermore, we investigate the effects of spin-orbit and spin-spin interactions. Based on these results we (i) explain quantitatively the spin polarization mechanism in experiments, (ii) find the zero-field splitting, in good agreement with experiment, (iii) present a mechanism that allows this defect to be used for electric field or strain sensing, and (iv) propose two spin-photon interface protocols enabled by the rich electronic structure of this defect, including the generation of strings of entangled photons and the creation of a Lambda system with

Orbital	S	m_s	Γ	$\Gamma_o \otimes \Gamma_s$	Symmetry adapted total wave functions	Label
ve^2 (Ground) & ue^2 (q1)	$\frac{3}{2}$	$\pm\frac{3}{2}$	$^1E_{3/2}$	$A_2 \otimes {}^2E_{3/2}$	$\|ve_xe_y + i\bar{v}\bar{e}_x\bar{e}_y\rangle/\sqrt{2}$	Ψ_{g}^1
			$^2E_{3/2}$	$A_2 \otimes {}^1E_{3/2}$	$\|ve_xe_y - i\bar{v}\bar{e}_x\bar{e}_y\rangle/\sqrt{2}$	Ψ_{g}^2
		$+\frac{1}{2}$	$E_{1/2}^+$	$A_2 \otimes E_{1/2}$	$\|ve_x\bar{e}_y + v\bar{e}_xe_y + \bar{v}e_xe_y\rangle/\sqrt{3}$	Ψ_{g}^3
		$-\frac{1}{2}$	$E_{1/2}^-$		$\|\bar{v}\bar{e}_xe_y + \bar{v}e_x\bar{e}_y + v\bar{e}_x\bar{e}_y\rangle/\sqrt{3}$	Ψ_{g}^4
e^3 (d1)	$\frac{1}{2}$	$+\frac{1}{2}$	$E_{1/2}^+$	$E \otimes E_{1/2}$	$\|e_x\bar{e}_xe_y + ie_y\bar{e}_ye_x\rangle/\sqrt{2}$	Ψ_{d1}^1
		$-\frac{1}{2}$	$E_{1/2}^-$		$\|\bar{e}_xe_x\bar{e}_y - i\bar{e}_ye_y\bar{e}_x\rangle/\sqrt{2}$	Ψ_{d1}^2
		$\pm\frac{1}{2}$	$^1E_{3/2}$		$\|(e_x\bar{e}_xe_y - ie_y\bar{e}_ye_x) - i(\bar{e}_xe_x\bar{e}_y + i\bar{e}_ye_y\bar{e}_x)\rangle/2$	Ψ_{d1}^3
			$^2E_{3/2}$		$\|(e_x\bar{e}_xe_y - ie_y\bar{e}_ye_x) + i(\bar{e}_xe_x\bar{e}_y + i\bar{e}_ye_y\bar{e}_x)\rangle/2$	Ψ_{d1}^4
ve^2 (d2)	$\frac{1}{2}$	$+\frac{1}{2}$	$E_{1/2}^+$	$A_2 \otimes E_{1/2}$	$\|ve_x\bar{e}_y + v\bar{e}_xe_y - 2\bar{v}e_xe_y\rangle/\sqrt{6}$	Ψ_{d2}^1
		$-\frac{1}{2}$	$E_{1/2}^-$		$\|\bar{v}\bar{e}_xe_y + \bar{v}e_x\bar{e}_y - 2v\bar{e}_x\bar{e}_y\rangle/\sqrt{6}$	Ψ_{d2}^2
ve^2 (d3)	$\frac{1}{2}$	$\pm\frac{1}{2}$	$^1E_{3/2}$	$E \otimes E_{1/2}$	$\|(ve_x\bar{e}_y - v\bar{e}_xe_y) - i(\bar{v}\bar{e}_xe_y - \bar{v}e_x\bar{e}_y)$ $+i(ve_x\bar{e}_x - ve_y\bar{e}_y) - (\bar{v}\bar{e}_xe_x - \bar{v}\bar{e}_ye_y)\rangle/2\sqrt{2}$	Ψ_{d3}^1
			$^2E_{3/2}$		$\|(ve_x\bar{e}_y - v\bar{e}_xe_y) + i(\bar{v}\bar{e}_xe_y - \bar{v}e_x\bar{e}_y)$ $+i(ve_x\bar{e}_x - ve_y\bar{e}_y) + (\bar{v}\bar{e}_xe_x - \bar{v}\bar{e}_ye_y)\rangle/2\sqrt{2}$	Ψ_{d3}^2
			$E_{1/2}^+$		$\|(ve_x\bar{e}_y - v\bar{e}_xe_y) - i(ve_x\bar{e}_x - ve_y\bar{e}_y)\rangle/2$	Ψ_{d3}^3
			$E_{1/2}^-$		$\|(\bar{v}\bar{e}_xe_y - \bar{v}e_x\bar{e}_y) + i(\bar{v}\bar{e}_xe_x - \bar{v}\bar{e}_ye_y)\rangle/2$	Ψ_{d3}^4
ve^2 (d4)	$\frac{1}{2}$	$+\frac{1}{2}$	$E_{1/2}^+$	$A_1 \otimes E_{1/2}$	$\|ve_x\bar{e}_x + ve_y\bar{e}_y\rangle/\sqrt{2}$	Ψ_{d4}^1
		$-\frac{1}{2}$	$E_{1/2}^-$		$\|\bar{v}\bar{e}_xe_x + \bar{v}\bar{e}_ye_y\rangle/\sqrt{2}$	Ψ_{d4}^2
v^2e (d5)	$\frac{1}{2}$	$+\frac{1}{2}$	$E_{1/2}^+$	$E \otimes E_{1/2}$	$\|v\bar{v}e_x - iv\bar{v}e_y\rangle/\sqrt{2}$	Ψ_{d5}^1
		$-\frac{1}{2}$	$E_{1/2}^-$		$\|\bar{v}v\bar{e}_x + i\bar{v}v\bar{e}_y\rangle/\sqrt{2}$	Ψ_{d5}^2
		$\pm\frac{1}{2}$	$^1E_{3/2}$		$\|(v\bar{v}e_x + iv\bar{v}e_y) + i(\bar{v}v\bar{e}_x - i\bar{v}v\bar{e}_y)\rangle/2$	Ψ_{d5}^3
			$^2E_{3/2}$		$\|(v\bar{v}e_x + iv\bar{v}e_y) - i(\bar{v}v\bar{e}_x - i\bar{v}v\bar{e}_y)\rangle/2$	Ψ_{d5}^4
uve (q2)	$\frac{3}{2}$	$+\frac{3}{2}$	$E_{1/2}$	$E \otimes {}^1E_{3/2}$	$\|uve_x\rangle\,,\ \|uve_y\rangle$	$\Psi_{\mathrm{q2}}^1, \Psi_{\mathrm{q2}}^2$
		$-\frac{3}{2}$	$E_{1/2}$	$E \otimes {}^2E_{3/2}$	$\|\bar{u}\bar{v}\bar{e}_x\rangle\,,\ \|\bar{u}\bar{v}\bar{e}_y\rangle$	$\Psi_{\mathrm{q2}}^3, \Psi_{\mathrm{q2}}^4$
		$\pm\frac{1}{2}$	$E_{1/2}^+$	$E \otimes E_{1/2}$	$\|(uv\bar{e}_y + u\bar{v}e_y + \bar{u}ve_y) + i(uv\bar{e}_x + u\bar{v}e_x + \bar{u}ve_x)\rangle/\sqrt{6}$	Ψ_{q2}^5
			$E_{1/2}^-$		$\|(\bar{u}\bar{v}e_y + \bar{u}v\bar{e}_y + u\bar{v}\bar{e}_y) - i(\bar{u}\bar{v}e_x + \bar{u}v\bar{e}_x + u\bar{v}\bar{e}_x)\rangle/\sqrt{6}$	Ψ_{q2}^6
			$^1E_{3/2}$		$\|(uv\bar{e}_y + u\bar{v}e_y + \bar{u}ve_y) - i(u\bar{v}\bar{e}_y + \bar{u}v\bar{e}_y + \bar{u}\bar{v}e_y)$ $-i(uv\bar{e}_x + u\bar{v}e_x + \bar{u}ve_x) + (u\bar{v}\bar{e}_x + \bar{u}v\bar{e}_x + \bar{u}\bar{v}e_x)\rangle/2\sqrt{3}$	Ψ_{q2}^7
			$^2E_{3/2}$		$\|(uv\bar{e}_y + u\bar{v}e_y + \bar{u}ve_y) + i(u\bar{v}\bar{e}_y + \bar{u}v\bar{e}_y + \bar{u}\bar{v}e_y)$ $-i(uv\bar{e}_x + u\bar{v}e_x + \bar{u}ve_x) - (u\bar{v}\bar{e}_x + \bar{u}v\bar{e}_x + \bar{u}\bar{v}e_x)\rangle/2\sqrt{3}$	Ψ_{q2}^8

TABLE I. Negatively charged Si vacancy wave functions for various configurations in the three hole representation. The states are classified in terms of orbital electronic configuration, total spin (S) and spin projection along the C_3-axis (m_s), overall symmetry representation of the state (Γ) and its decomposition in terms of the orbital and spin symmetries ($\Gamma_o \otimes \Gamma_s$). q1 states (not explicitly shown) are defined similarly to states Ψ_{g}^1-Ψ_{g}^4 with the replacement $v \to u$. The notation $\|\ldots\rangle$ represents the Slater determinant of each component inside the bracket. The bar (no bar) over an orbital indicates spin down (up).

potential applications in quantum technologies.

The $C_{6\nu}$ symmetry of bulk 4H-SiC is lowered to the $C_{3\nu}$ point group in the presence of $\mathrm{V_{Si}^-}$. The local geometry of $\mathrm{V_{Si}^-}$ is shown in Fig. 1(a), where the missing silicon leaves four dangling bonds (sp^3-orbitals) on the surrounding carbons [27]. Single electron molecular orbitals (MO) can be constructed from symmetry-adapted linear combinations of the three equivalent sp^3-orbitals (a, b and c) from the basal-plane carbons and the sp^3-orbital,

d, belonging to the carbon atom on the C_3-axis that coincides with the crystalline c-axis. Using the standard projection operator technique [28] and our DFT results as a guide [Fig. 1(b)-(d)], we obtain the following MOs of the defect center: $u = \alpha_u(a+b+c) + \beta_u d$, $v = \alpha_v(a+b+c) + \beta_v d$, $e_x = \alpha_x(2c - a - b)$, and $e_y = \alpha_y(a - b)$, where the coefficients are given in [29]. The orbitals, as calculated by DFT [30–32], are shown in Fig.1. The functions u and v transform as A_1, e_X and e_Y transform as the x and y

components of the E representation respectively and the states are listed in order of increasing energy according to our DFT calculations.

The electronic configuration of this defect is modeled by three holes, a simpler but equivalent picture to that of five active electrons. Then, the three-hole lowest energy quartet configurations are identified as ve_xe_y, ue_xe_y, and uve_x (or uve_y), respectively, increasing in energy [29]. The tensor products of u, v, and $e_{x,y}$ states with the total spin eigenstates comprise our basis set, from which we calculate the multi-particle symmetry-adapted states compatible with C_{3v}. The odd number of particles and the symmetry only slightly broken from T_d here results in a complicated electronic and spin structure different than those of NV$^-$ or NV^0 centers [33, 34] in diamond and divacancies in SiC. Thus, we obtain the multi-particle wave functions systematically by use of the projection operator on the basis states for both the orbital and the spin degree of freedom:

$$\mathcal{P}^{(j)} = (I_j/h)\sum_R \chi^{(j)}(R)^*\Gamma^{(j)}(R), \qquad (1)$$

where, $\chi^{(j)}(R)$ is the character of operation R in the jth irreducible representation [29], and Γ is the irreducible matrix representation for the R symmetry operator (tensor product of the three-particle orbital and spin operators [29]). The resulting symmetry adapted states are shown in Table I, and are characterized by the total spin S, the orbital and spin symmetry, as well as their overall symmetry. These classifications are of key importance in understanding the nature of these states, their additional interactions, as well as the allowed optical or spin-orbit assisted transitions and selection rules. The ground state manifold has $S=3/2$ (quartet), while there are nearby additional manifolds (each a doublet, $S=1/2$) with some having the same orbital composition as the ground state and split from each other only due to Coulomb interactions (see Fig. 3 and [29]).

The states are split and mixed further by spin-orbit (SO) and spin-spin interactions. The SO coupling is

$$\mathcal{H}_{SO} = \sum_j \boldsymbol{\ell}_j \cdot \boldsymbol{s}_j, \qquad (2)$$

where ℓ_j and s_j are orbital and spin angular momentum operators belonging to the jth hole. The former is defined as $(\ell_j)_i = \epsilon_{ikl}[\nabla V(\boldsymbol{r}_j)]_k[\boldsymbol{p}_j]_l/2m^2c^2$ where the $V(\boldsymbol{r_j})$ is the local potential, $\boldsymbol{p_j}$ is the hole momentum operator with coordinate indices i, k, l. The components of both ℓ and $\mathbf{s}$ transform as the (E_Y, E_X, A_2) representation and the H_{SO} Hamiltonian itself transforms as A_1. With these symmetry classifications we see that the diagonal part of H_{SO}, $\sum_j \ell_{j,z}s_{j,z}$, will only couple states of the same L and S and of orbital symmetry E (since $A_1\subset E\otimes A_2\otimes E$). Thus, the

ground states do not split due to this term, while states $\{\Psi_d^j\}$ and $\{\Psi_{q2}^j\}$ shift and/or mix within their manifolds, as shown in Fig. 2 by $\Delta_d=\langle\phi_\xi^E||L_z^{A_2}||\phi_\xi^E\rangle/(2\sqrt{2})$ and $\Delta_q=\langle\phi_{uve}^E||L_z^{A_2}||\phi_{uve}^E\rangle/(2\sqrt{2})$ respectively (given in terms of reduced matrix elements and $\xi = \{e^3, v^2e\}$). Note that the total orbital angular momentum operator is used here, which is equivalent to using Eq. 2 for matrix elements between states of the same total S and L [28].

The transverse parts of the SO interaction, $\sum_j \ell_{j,\perp}s_{j,\perp}$, couple states of different total spin and orbital character $\{u, v\}$ to both e_x and e_y at single particle level. Hence the ground states will couple to $\{\Psi_{d1}^j\}$ (defined in Table I) via these transverse SO terms. This coupling is crucial both in explaining existing experiments and in designing future applications. The key is to notice that ground states and q1 excited states with $|S_z|=3/2$ couple more strongly to excited $\{\Psi_{d1}^j\}$ (e^3) states compared to the states with $|S_z|=1/2$. In fact using the states of Table I we can show that the ratio of the matrix elements is $\sqrt{3}$. From this we identify the dominant intersystem crossing channel that constitutes the spin polarization mechanism seen in recent experiments at the single-spin level [17] with h-site (V_2) defects, where optical driving polarizes the system into the $|S_z|=3/2$ states. This mechanism, shown in Fig. 3, also successfully predicts the recently seen increase in the ODMR photo-luminescence intensity with microwave drive [8, 15, 17, 18, 20].

We can also consider first-order perturbing corrections to the ground state wave functions from the excited dark doublet states through spin-orbit coupling (see Fig. 3). The different strength of the SO matrix elements (e.g., the extra involvement of $l_{j,z}s_{j,z}$ with $m_s = \pm 1/2$ states only) will cause a different degree of admixture of excited states to the $|S_z|=3/2$ and $|S_z|=1/2$ ground states, which in turn will allow an electric field [35], strain and mechanical motion [36–38] to couple ground states with different $|S_z|$ projections. This paves the way toward unexplored SiC-based applications in sensing.

Next we consider the spin-spin interaction between the holes. The Hamiltonian is

$$\mathcal{H}_S = \frac{\mu_0 g^2 \mu_B^2}{4\pi}\sum_{i>j}\frac{1}{r_{ij}^3}\left\{\boldsymbol{s}_i\cdot\boldsymbol{s}_j - 3\left(\boldsymbol{s}_i\cdot\hat{\boldsymbol{r}}_{ij}\right)\left(\boldsymbol{s}_j\cdot\hat{\boldsymbol{r}}_{ij}\right)\right\},$$

$$(3)$$

where g is the electron g-factor, μ_0 is the vacuum permeability, and μ_B is the Bohr magneton. The spin operator of each hole, the distance to each other and its unit vector are s_i, r_{ij} and $\hat{\boldsymbol{r}}_{ij}$, respectively. The spin-spin splittings of the quartets and doublets are shown in Fig. 2 in terms of the splitting parameters defined as $\gamma_g=\gamma_0\langle\phi_{ve^2}^{A_2}||I_2||\phi_{ve^2}^{A_2}\rangle/\sqrt{10}$, $\gamma_{q1}=\gamma_0\langle\phi_{ue^2}^{A_2}||I_2||\phi_{ue^2}^{A_2}\rangle/\sqrt{10}$, $\gamma_d=\gamma_0\langle\phi_\xi^E||I_2||\phi_\xi^E\rangle/(6\sqrt{10})$, $\gamma_{q2}^1=\gamma_0\langle\phi_{uve}^E||I_2||\phi_{uve}^E\rangle/(2\sqrt{10})$ and $\gamma_{q2}^2=\gamma_{q2}^1(1 - 1.028\zeta)$, where I_2 is an irregular solid harmonic of second rank,
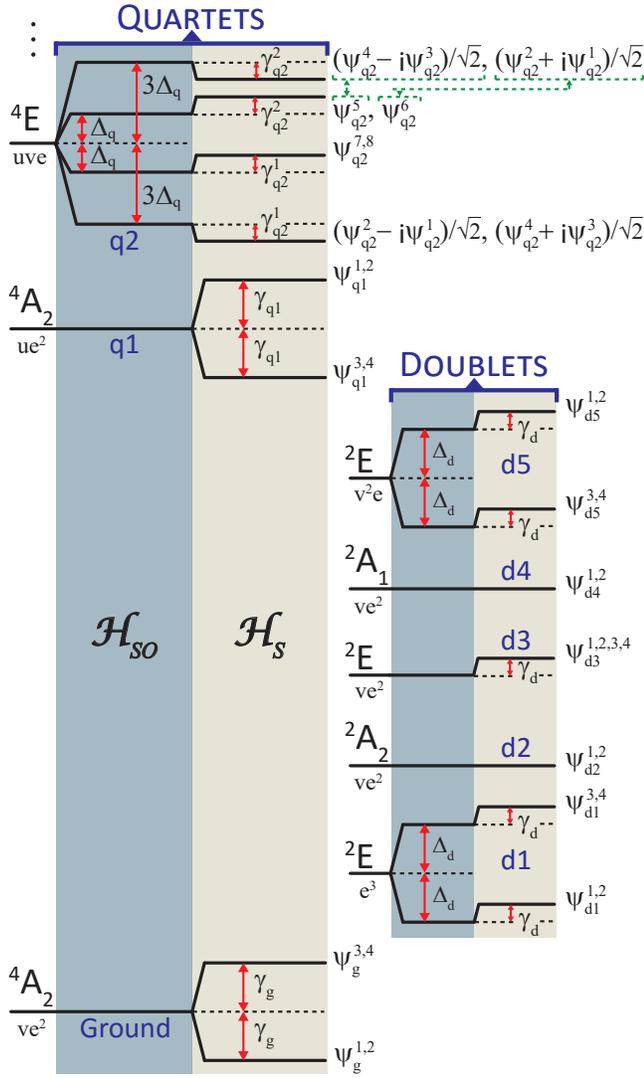
FIG. 2. (color online) Electronic configuration of V_{Si}^-, shown in terms of the wave functions given in Table I. The splittings are shown explicitly for the SO and spin-spin interactions. The spin quartets are grouped on the left half whereas the metastable doublets are on the right. The states with subscript q and d denote excited quartet and doublet states, respectively. The dashed (green) arrows indicate the mixing due to spin-spin interactions.

i.e. $I_l^m = \sqrt{4\pi/(2l+1)} Y_l^m/r^{l+1}$, $\gamma_0 = \mu_0 g^2 \mu_B^2/4\pi$, and $\zeta = \langle \phi_{uve}^E || I_2 || \phi_{uve}^E \rangle / \Delta_q \approx 0$, see [29]. Using in these expressions the calculated bond lengths $d=2.058$ Å, $a=2.055$ Å, and $\theta_0 = 35.26°$ from our DFT results, we estimate the zero field splitting (ZFS) to be $2|\gamma_g|=68$ MHz, in good agreement with experiments [13, 15, 18, 20]. However, we found a negative D for the ground state, i.e. $\mathcal{H}_S \simeq D[S_z^2 - S(S+1)/3]$, causing $m_s = \pm 1/2$ to be energetically higher than the $m_s = \pm 3/2$ states contrary to the some assumptions of $D>0$ in literature. In the limit of perfect tetrahedral (T_d) symmetry, our calculation also leads to a vanishing ZFS (0 MHz) consistent
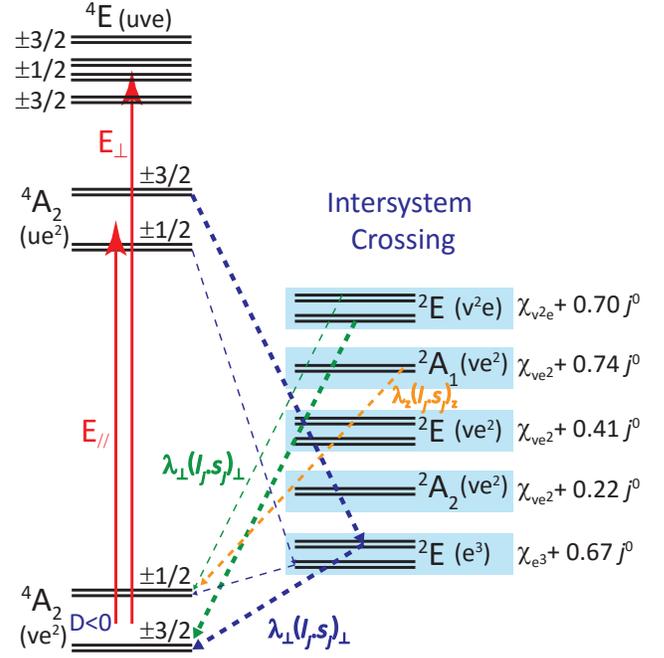
FIG. 3. (color online) Spin polarization channel of V_{Si}^- through the spin-orbit assisted dominant intersystem crossing $^4A_2(ue^2) \rightarrow {}^2E(e^3) \rightarrow {}^4A_2(ve^2)$ and all other allowed channels are shown in dashed lines. Thicker lines of blue and green indicate $3\times$ faster transition rate from or to $m_s = \pm 3/2$ states by the transverse component of spin-orbit $\lambda_\perp$ whereas orange represents a channel via the longitudinal λ_z component. Energies of the doublets are ordered in terms of the one-particle Coulomb Hamiltonian $\chi = \langle \phi | \sum h_i | \phi \rangle$ and leading many-particle direct integrals [39], i.e. $j^0 = \int \rho_{aa}(r_1) V_R(r_1, r_2) \rho_{aa}(r_2) d^3 r_1 d^3 r_2$, of Coulomb repulsion [29].

with the lack of any ZFS with V_{Si}^- centers in 3C-SiC.

Based on Table I, the rich structure of the various transitions and immunity to all local perturbing electric and strain fields (Kramer's degeneracy) enable the design of a spin-photon interface for applications in quantum computing and quantum communications. Below we propose two such protocols. First consider the ground states with $|S_z|=3/2$, split by a B-field along the C_3 axis, $\Psi_g^\pm = \Psi_g^1 \pm \Psi_g^2$. The excited states of interest are $\Psi_e^+ = \Psi_{q2}^2 - i\Psi_{q2}^1$ and $\Psi_e^- = \Psi_{q2}^4 + i\Psi_{q2}^3$, which are degenerate energy eigenstates after SO has been included (Fig. 2); these states have $|S_z|=3/2$, and since the g-factor is the same in ground and excited states [24] they split by the same amount as the lower levels. They are also the only states which are not coupled to the states of $^4A_2$ q1 manifold via $\sum_j \ell_{j,\perp} s_{j,\perp}$ terms. The allowed optical transitions between these sets of states are $\Psi_g^+ \leftrightarrow \Psi_e^+$ and $\Psi_g^- \leftrightarrow \Psi_e^-$ with right and left circularly polarized light respectively, Fig. 4(a). A coherently excited superposition of the two excited states decays to an entangled spin-photon state, $|\Psi_g^+\rangle|\sigma+\rangle + |\Psi_g^-\rangle|\sigma-\rangle$. Repeating this process produces additional photons, all en-

tangled with the spin and each other, resulting in a multiphoton Greenberger-Horne-Zeilinger state. Augmenting the optical protocol with microwaves can couple the ground states and allow the production of a cluster state [40], similarly to a proposal for quantum dots [41, 42].

Next we consider a B-field perpendicular to the C_3 axis. This mixes all four ground states, and from these we select Ψ_g^α and Ψ_g^β, along with the excited state Ψ_e^γ (all of them given in [29] in terms of the states of Table I). Then a Λ-system can be formed, Fig. 4(b). This three-level system can be used in numerous quantum applications and demonstrations, including coherent population trapping [43], optical spin qubit rotations [44, 45] and generation of spin-photon entanglement [2, 46] with applications in quantum repeaters [47].
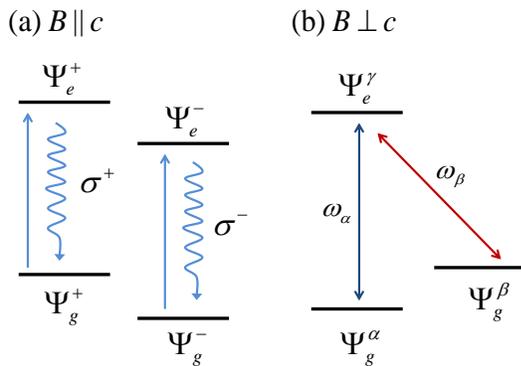
FIG. 4. (color online) (a) A B-field parallel to the C_3 axis enables the creation of two two-level systems with the same transition frequency but orthogonal polarizations. Periodic coherent pumping followed by spontaneous emission leads to strings of entangled photons. (b) A B-field perpendicular to the C_3 axis allows for the creation of a Lambda system.

In summary, we addressed the crucial need of calculating the multi-particle fine structure of the silicon vacancy defect in SiC. Based on the resulting spectrum we identified the intersystem crossing channel that polarizes the system, found a mechanism to enable quantum sensing applications, and proposed two spin-photon interface protocols. Our work opens further opportunities in understanding these defects and in implementing novel quantum technological applications.

[1] E. Togan, Y. Chu, A. Imamoglu, and M. D. Lukin, Nature **478**, 497 (2011).

[2] H. Bernien, B. Hensen, W. Pfaff, G. Koolstra, M. S. Blok, L. Robledo, T. H. Taminiau, M. Markham, D. J. Twitchen, L. Childress, et al., Nature **497**, 86 (2013).

[3] M. S. Grinolds, S. Hong, P. Maletinsky, L. Luan, M. D. Lukin, R. L. Walsworth, and A. Yacoby, Nature Physics **9**, 215 (2013).

[4] G. Balasubramanian, I. Y. Chan, R. Kolesov, M. Al-Hmoud, J. Tisler, C. Shin, C. Kim, A. Wojcik, P. R. Hemmer, A. Krueger, et al., Nature **455**, 648 (2008).

[5] F. Shi, Q. Zhang, P. Wang, H. Sun, J. Wang, X. Rong, M. Chen, C. Ju, F. Reinhard, H. Chen, et al., Science **347**, 1135 (2015).

[6] B. S. Song, S. Yamada, T. Asano, and S. Noda, Opt. Express **19**, 11084 (2011).

[7] R. Maboudian, C. Carraro, D. G. Senesky, and C. S. Roper, J. Vac. Sci. Technol. A **31**, 50805 (2013).

[8] P. G. Baranov, A. P. Bundakova, A. A. Soltamova, S. B. Orlinskii, I. V. Borovykh, R. Zondervan, R. Verberk, and J. Schmidt, Phys. Rev. B. **83**, 125203 (2011).

[9] N. T. Son, P. Carlsson, J. Hassan, E. Janzén, T. Umeda, J. Isoya, A. Gali, M. Bockstedte, N. Morishita, T. Ohshima, et al., Phys. Rev. Lett. **96**, 055501 (2006).

[10] W. F. Koehl, B. B. Buckley, F. J. Heremans, G. Calusine, and D. D. Awschalom, Nature **479**, 84 (2011).

[11] A. L. Falk, B. B. Buckley, G. Calusine, W. F. Koehl, V. V. Dobrovitski, A. Politi, C. A. Zorman, P. X.-L. Feng, and D. D. Awschalom, Nat. Commun. **4**, 1819 (2013).

[12] D. J. Christle, A. L. Falk, P. Andrich, P. V. Klimov, J. U. Hassan, N. T. Son, E. Janzén, T. Ohshima, and D. D. Awschalom, Nat. Mater. **14**, 160 (2014).

[13] N. Mizuochi, S. Yamasaki, H. Takizawa, N. Morishita, T. Ohshima, H. Itoh, and J. Isoya, Phys. Rev. B **66**, 235202 (2002).

[14] D. Riedel, F. Fuchs, H. Kraus, S. Väth, A. Sperlich, V. Dyakonov, A. A. Soltamova, P. G. Baranov, V. A. Ilyin, and G. V. Astakhov, Phys. Rev. Lett. **109**, 226402 (2012).

[15] H. Kraus, V. A. Soltamov, D. Riedel, S. Väth, F. Fuchs, A. Sperlich, P. G. Baranov, V. Dyakonov, and G. V. Astakhov, Nature Physics **10**, 157 (2014).

[16] H. Kraus, V. A. Soltamov, F. Fuchs, D. Simin, A. Sperlich, P. G. Baranov, G. V. Astakhov, and V. Dyakonov, Sci. Rep. **4**, 5303 (2014).

[17] M. Widmann, S.-Y. Lee, T. Rendler, N. T. Son, H. Fedder, S. Paik, N. Z. L.-P. Yang, S. Yang, I. Booker, A. Denisenko, et al., Nat. Mater. **14**, 164 (2015).

[18] S. G. Carter, O. O. Soykal, P. Dev, S. E. Economou, and E. R. Glaser, Phys. Rev. B **92**, 161202(R) (2015).

[19] V. A. Soltamov, A. A. Soltamova, P. G. Baranov, and I. I. Proskuryakov, Phys. Rev. Lett. **108**, 226402 (2012).

[20] E. Sörman, N. T. Son, W. M. Chen, O. Kordina, C. Hallin, and E. Janzén, Phys. Rev. B **61**, 2613 (2000).

[21] A. Lenef and S. C. Rand, Phys. Rev. B **53**, 13441 (1996).

[22] J. R. Maze, A. Gali, E. Togan, Y. Chu, A. Trifonov, E. Kaxiras, and M. D. Lukin, New Journal of Physics **13**, 025025 (2011).

[23] M. W. Doherty, N. B. Manson, P. Delaney, and L. C. L. Hollenberg, New J. Phys. **13**, 025019 (2011).

[24] E. Janzén, A. Gali, P. Carlsson, A. Gllström, B. Magnusson, and N. T. Son, Physica B **404**, 4354 (2009).

[25] J. R. Weber, W. F. Koehl, J. B. Varley, A. Janotti, B. B. Buckley, C. G. V. de Walle, and D. D. Awschalom, Proc. Natl. Acad. Sci. **107**, 8513 (2010).

[26] A. Gali, Journal of Materials Research **27**, 897 (2012).

[27] E. Hückel, Zeitschrift für Physik **70**, 204 (1931).

[28] M. Tinkham, *Group Theory and Quantum Mechanics* (Dover, New York, 2003).

[29] See supplement.

[30] P. Giannozzi, S. Baroni, N. Bonini, M. Calandra, R. Car, C. Cavazzoni, D. Ceresoli, G. L. Chiarotti, M. Cococcioni, I. Dabo, et al., Journal of Physics: Condensed Matter **21**, 395502 (19pp) (2009), URL `http://www.quantum-espresso.org`.

[31] J. P. Perdew and Y. Wang, Phys. Rev. B **33**, 8800 (1986).

[32] J. P. Perdew, K. Burke, and M. Ernzerhof, Phys. Rev. Lett. **77**, 3865 (1996).

[33] S. Felton, A. M. Edmonds, M. E. Newton, P. M. Martineau, D. Fisher, and D. J. Twitchen, Phys. Rev. B **77**, 081201(R) (2008).

[34] A. Gali, Phys. Rev. B **79**, 235210 (2009).

[35] F. Dolde, H. Fedder, M. W. Doherty, T. Nöbauer, F. Rempp, G. Balasubramanian, T. Wolf, F. Reinhard, L. C. L. Hollenberg, F. Jelezko, et al., Nature Physics **7**, 459 (2011).

[36] O. O. Soykal, R. Ruskov, and C. Tahan, Phys. Rev. Lett. **107**, 235502 (2011).

[37] S. Hong, M. S. Grinolds, P. Maletinsky, R. L. Walsworth, M. D. Lukin, and A. Yacoby, Nano Lett. **12 (8)**, 3920 (2012).

[38] E. R. MacQuarrie, T. A. Gosavi, N. R. Jungwirth, S. A. Bhave, and G. D. Fuchs, Phys. Rev. Lett. **111**, 227602 (2013).

[39] G. D. Mahan, *Many-particle Physics* (Kluwer Academic, New York, 2000).

[40] R. Raussendorf and H. J. Briegel, Phys. Rev. Lett. **86**, 5188 (2001).

[41] N. H. Lindner and T. L. Rudolph, Phys. Rev. Lett. **103**, 113602 (2009).

[42] S. E. Economou, N. H. Lindner, and T. L. Rudolph, Phys. Rev. Lett. **105**, 093601 (2010).

[43] C. Santori, D. Fattal, S. M. Spillane, M. Fiorentino, R. G. Beausoleil, A. D. Greentree, P. Olivero, M. Draganski, J. R. Rabeau, P. Reichart, et al., Optics Express **14**, 7986 (2006).

[44] S. E. Economou and T. L. Reinecke, Phys. Rev. Lett. **99**, 217401 (2007).

[45] C. G. Yale, B. B. Buckley, D. J. Christle, G. Burkard, F. J. Heremans, L. C. Bassett, and D. D. Awschalom, Proc. Natl. Acad. Sci. **110**, 7595 (2013).

[46] E. Togan, Y. Chu, A. S. Trifonov, L. Jiang, J. Maze, L. Childress, M. V. G. Dutt, A. S. Sørensen, P. R. Hemmer, A. S. Zibrov, et al., Nature **730**, 84 (2010).

[47] H. J. Briegel, W. Dür, J. I. Cirac, and P. Zoller, Phys. Rev. Lett. **81**, 5932 (1998).